

RESEARCH

Open Access



Experimental Investigation of Inclusion of Various Nanocarbon Black Concentrations on Mechanical Characteristics of Oil-Well Cement Slurries in High-Pressure High-Temperature Conditions

Ahmed Ebied^{1,3*} , Sherif Fakher² and Hatem Kayed¹

Abstract

This study investigates the impact of adding nanocarbon black (NCB) to wellbore cement under high-pressure, high-temperature (HPHT) conditions to enhance its properties for long-term zonal isolation. Four cementitious slurries were prepared in the laboratory using the wet-mixing method, following the American Petroleum Institute standards (API 10B-2 and API 10A). NCB was incorporated as a reinforced nanomaterial in cementitious composites at varying concentrations of 0.05%, 0.1%, and 0.2% by weight of cement (BWOC) into the slurry mix fluid following a specific mixing sequence before the addition of Class-G wellbore Portland cement, which is manufactured via the dry process and commonly used in the oil and gas industry. The study evaluated parameters, such as density, rheology, free fluid (FF), fluid loss (FL), thickening time (TT), compressive strength (CS), tensile strength (TS), porosity, and permeability, following API standards. The results demonstrated that NCB additions slightly increased slurry density and significantly improved rheological properties, with low yield stress at bottomhole circulating temperatures. NCB concentrations of 0.05% and 0.1% reduced free fluid, fluid loss, and thickening time while enhancing the cement sheath's compressive and tensile strength, simultaneously reducing its porosity and permeability. Moreover, the improved early compressive strength development indicated accelerated cement hydration reactions due to incorporating NCB. The study found that 0.1% NCB was the optimal concentration, enhancing mechanical properties and operational efficiency by reducing wait-on-cement time and costs while improving wellbore integrity. However, higher NCB concentrations required careful dispersion to prevent nanoparticle agglomeration. Overall, NCB significantly enhanced cement sheath characteristics under HPHT conditions.

Keywords Nanocarbon black, HPHT wellbore integrity, Rheological properties, Mechanical characteristics, Porosity, Permeability

*Correspondence:

Ahmed Ebied

Ahmed.Ebied.J@eng-st.cu.edu.eg

¹ Department of Power Mechanical Engineering, Faculty of Engineering, Cairo University, Cairo, Egypt

² Department of Petroleum and Energy Engineering, Faculty of Engineering, The American University in Cairo, Cairo, Egypt

³ Department of Well Construction Fluids, Egypt Center of Efficiency, SLB, Cairo, Egypt

1 Introduction

Wellbore cementing is an essential operation throughout both the drilling and the production phases. The main objective of primary cement is to create a barrier separating the casing from the surrounding formation to support the casing and provide zonal isolation by preventing the fluid's communication throughout all wellbore formations during the wellbore lifetime

(Alkhamis & Imqam, 2018). The cementing operations in thermal wells or exploration of new reserves in challenging environments such as HPHT conditions lead to cyclic thermal stresses on the cement sheath that can result in wellbore cementing failures such as microannuli and severe cracks and might cause compromised zonal isolation that can endanger equipment, personnel, and the environment, and increase the number of remedial cementing jobs which would, in turn, increase the costs of the production phase to overcome these issues to prevent the complete loss of the well (Nelson & Guillot, 2016; Helmy, Y. and Fakher, S., 2024). Even with the recent progress in advanced smart polymeric materials, fibers, and self-healing materials, achieving sufficient long-term zonal isolation in harsh oil well conditions remains a significant challenge (Jafariesfad et al., 2017). Consequently, it is important to find a new approach to designing a cement system capable of enduring the potentially severe conditions throughout the wellbore life cycle. Nanotechnology offers a promising approach to transforming conventional cement systems into unconventional, durable, flexible cement systems that are capable of withstanding imposed mechanical and thermal stressful conditions (Deshpande and Patil 2017, Jimenez et al., 2016, Fakher, S. et al., 2023a; 2023b). Incorporating nanocarbon-based materials represents a promising method for enhancing the short-term and long-term performance of cement sheaths in wellbore cementing operations (Fakher, S. and Khlaifat, A., 2023; Khlaifat, A. et al., 2024). Wu et al. (2024) analyzed the microstructure, pore structure, and electromagnetic properties of cement paste with nanocarbon black (CB), revealing that the incorporation of CB enhanced the pore structure by increasing the proportion of small pores (<100 nm) and improving overall pore distribution. Although the presence of CB agglomerates initially decreased compressive strength, the use of dispersant at 0.5 wt% CB effectively reduced the size of the agglomerates and significantly increased compressive strength. Sridhar et al., (2024a, 2024b) investigated the mechanical properties of hybrid fiber-reinforced concrete (HFRC) by evaluating compressive strength, split tensile strength, and flexural strength in mixtures with steel and polypropylene fibers at different volume fractions (0.25%, 0.5%, and 0.75%). The findings showed that the inclusion of fibers greatly improved the concrete's mechanical performance. Notably, the blend of steel fibers' high elastic modulus with polypropylene fibers' low elastic modulus proved especially beneficial in enhancing the concrete's overall strength and durability. Aosai et al. (2024) examined the impact of incorporating nanoalumina (1% to 3%) with polyvinyl alcohol (PVA) fibers and the hybridization of nanosilica (NS) and

nanoalumina (NA) were examined and results showed that hybrid nanoparticles greatly enhanced compressive strength compared to control and NA mortars. However, workability declined at higher concentrations. The optimal strength improvement of 7.4% was achieved with 0.5% NA and 2.5% NS. Nunes et al. (2014) investigated the effect of the addition of carbon nanotubes (CNTs) on the rheological and mechanical properties of cement slurries used in oil wells, and it was found that the inclusion of CNTs, at concentrations of 0.1% and 0.3% BWOC, did not affect the slurry's rheological behavior or stability. Souza et al. (2020) examined the influence of multiwall carbon nanotubes (MWCNTs) on Portland cement paste, and the findings revealed that MWCNTs accelerated the cement's hydration rate, shortened the initial setting time, and modified the hydration process, with more pronounced changes at higher concentrations (0.15% to 0.30% BWOC). Y. Li et al. (2021) investigated the reinforcement of wellbore cement using botryoid hybrid nanocarbon materials (BHNCMs) and found that a 1% BWOC concentration enhanced the cement's flexibility and strength by 20%. Peyvandi et al. (2017) examined the incorporation of low-cost graphite nanoplatelet (GNP) and carbon nanofibers (CNF) into cementitious materials to improve zonal isolation in oil and gas wells, and their findings indicated a 20% increase in flexural strength, a 10% increase in tensile strength, and a 50% enhancement in shrinkage resistance with only 0.2% GNP and CNF. Nochaiya and Chaipanich (2011) investigated the porosity of Portland cement composites incorporating up to 1% MWCNTs BWOC was investigated and found that the inclusion of MWCNTs decreased the total porosity of the cement sheath from 27.2% to 22.7%. Rezanian et al. (2019) studied the combined impact of nanocarbon black (NCB) and nanosilica on cement sheaths, revealing that these nanoparticles notably reduced the permeability of cement paste. G. Y. Li et al. (2005) and De La Roij et al. (2012) discovered that integrating nanomaterials into the calcium silicate hydrate (C-S-H) structure within cement matrices enhanced both strength and flexibility. This improvement was achieved by bridging tensile stresses and reinforcing the C-S-H structure, effectively preventing crack propagation. Singh and Vander Wal (2018) analyzed carbon blacks' lattice characteristics and nanoscale structure using transmission electron microscopy (TEM) due to its availability, low cost of use, and higher magnification capability than scanning electron microscopy (SEM). TEM images illustrating these diverse carbon blacks are presented in Fig. 1. The study found that nanostructure variations affect properties like surface area and color intensity, with finer particles providing better reinforcement. Carbon blacks are produced in various grades for different applications.

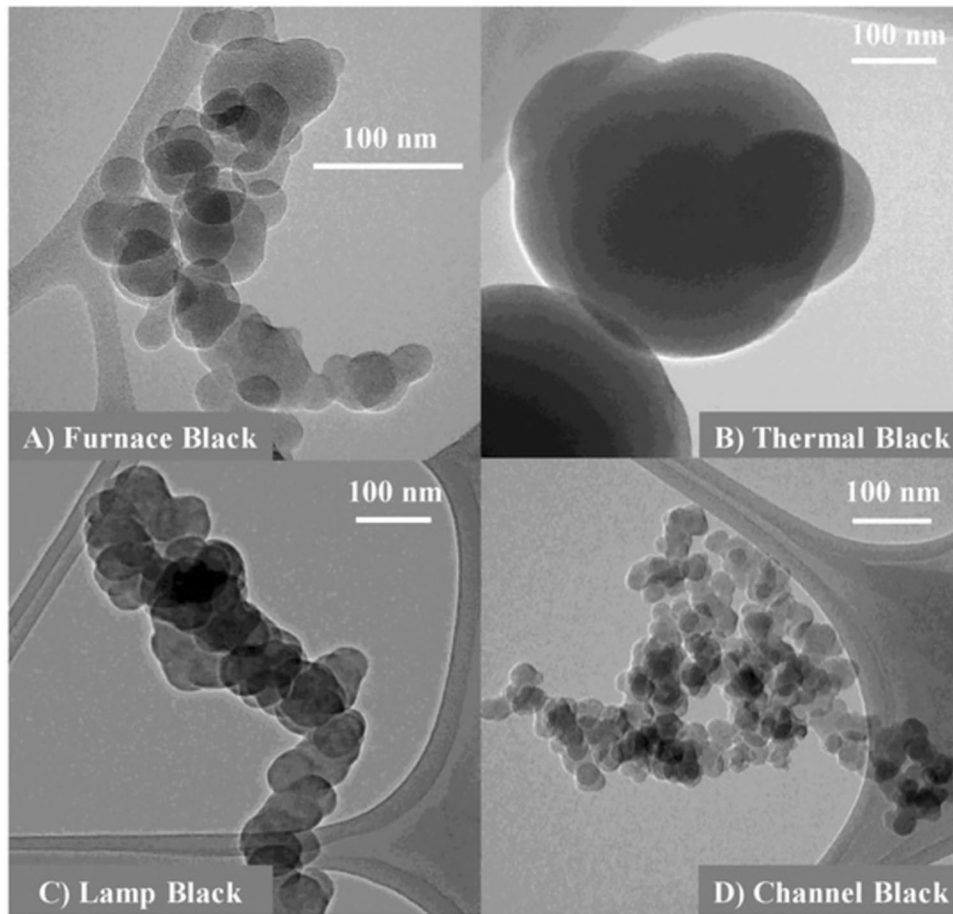


Fig. 1 TEM images showing aggregates of **A** furnace, **B** thermal, **C** lamp, and **D** channel blacks (Singh & Vander Wal, 2018)

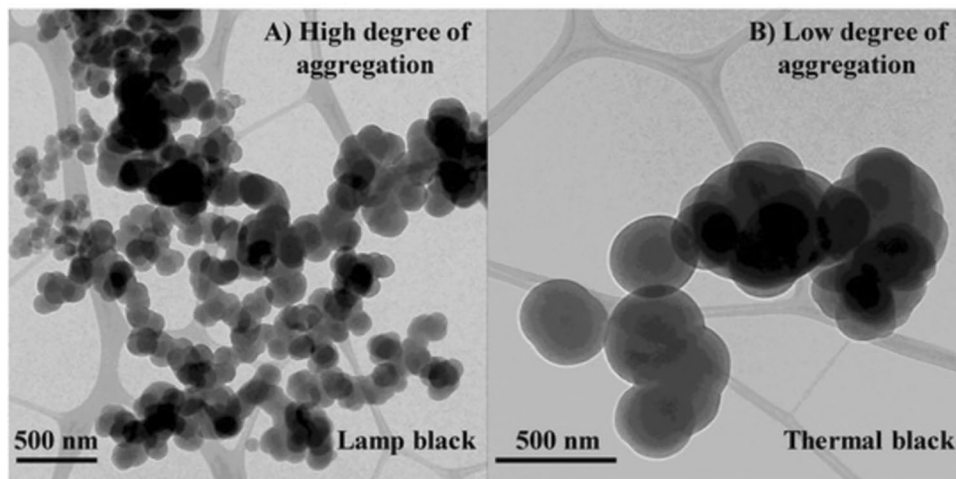


Fig. 2 TEM images contrasting **A** a high and **B** a low degree of aggregation in the different carbon blacks (Singh & Vander Wal, 2018)

Table 1 Chemical composition of Italian API Class-G Portland cement

| Chemical composition | Standard requirements | Sample results |
|---|--|----------------|
| | API Spec 10A (ISO 10426-1:2009) | |
| Loss on ignition, (max %) | 3.00 | 1.20 |
| Magnesium oxide, (max %) | 6.00 | 1.20 |
| Sulfur trioxide, (max %) | 3.00 | 2.50 |
| Insoluble residue, (max %) | 0.75 | 0.19 |
| Total alkali content (Na ₂ O), (max %) | 0.75 | 0.64 |
| Tricalcium silicate, (max %) | 48–65 | 51.00 |
| Tricalcium aluminate, (max %) | 3.00 | 0.50 |
| 2C ₃ A + C ₄ AF, (max %) | 24.00 | 16.70 |

Examples of carbon blacks with varying degrees of aggregation are shown in Fig. 2. Based on an extensive literature review that highlights the ongoing difficulties in achieving long-term zonal isolation and maintaining cement sheath integrity under harsh conditions. This study investigates the effectiveness of nanocarbon black (NCB) in enhancing wellbore cementing performance in high-pressure, high-temperature (HPHT) conditions. Also, it identifies the optimal concentrations needed to maximize these improvements through comprehensive experimentations by incorporating nanocarbon black (NCB) into Class-G Portland cement slurries to investigate the NCB's effects on a broad range of cement properties, including density, rheology, fluid behavior, mechanical strength, porosity, and permeability. This research's novelty lies in providing a new perspective on mitigating wellbore cementing failures in HPHT conditions and emphasizing the potential for developing cost-effective, environmentally sustainable solutions that can significantly enhance the sustainability and efficiency of oil and gas production operations.

2 Experimental

2.1 Materials

The study used Class-G Portland cement with high-sulfate-resistant grade (HSR), which is a common material for cementing in oil and gas wells. The cement's chemical composition and physical performance are detailed in Tables 1 and 2, respectively, which are typical for cements and materials for well cementing standard requirements (API 10A, 2019) to ensure proper hydration of cement and its validity for laboratory testing and field use for wellbore cementing operations. The nanomaterial used in the research is nanocarbon black (NCB) from Birla Carbon Inc. It is a black-gray spherical nanoparticle with

Table 2 Physical performance of Italian API Class-G Portland cement

| Physical performance | Standard requirements | Sample results |
|-----------------------|--|-----------------------|
| | API Spec 10A (ISO 10426-1:2009) | |
| Specific gravity | 3.15–3.2 g/cm ³ | 3.2 g/cm ³ |
| Setting time at 52 °C | 90–120 min | 111 min |
| Free fluids at 26 °C | 5.9% | 2.3% |
| CS, 8 h at 38 °C | ≥ 2.1 MPa | 3.93 MPa |
| CS, 8 h at 60 °C | ≥ 10.3 MPa | 13.39 MPa |

Table 3 Physical and chemical characteristics of NCB

| | |
|---|---|
| Particle size | 39–55 nm |
| Specific gravity | 1.92 g/cm ³ |
| Specific surface area | 39–41 m ² /g |
| Iodine absorption | 39–47 g/kg |
| DBP absorption | 116–126 (10 ⁻⁵ m ³ /kg) |
| Heat loss | 1.5% |
| Ash content (non-carbon/inorganic material) | 0.5% |

Table 4 Cement slurry compositions used in experiments based on API 10B-2

| Materials | C 1 | C 2 | C 3 | C 4 |
|-------------------------------------|------|------|------|------|
| Cement, %BWOC (Dyckerhoff) | 100 | 100 | 100 | 100 |
| Silica, %BWOC (SLB) | 35 | 35 | 35 | 35 |
| Antifoam, %BWOC (SLB) | 0.01 | 0.01 | 0.01 | 0.01 |
| Fluid loss agent, %BWOC (SLB) | 0.35 | 0.35 | 0.35 | 0.35 |
| Extender, %BWOC (SLB) | 7 | 7 | 7 | 7 |
| Dispersant, %BWOC (SLB) | 1.4 | 1.4 | 1.4 | 1.4 |
| Retarder, %BWOC (SLB) | 0.3 | 0.3 | 0.3 | 0.3 |
| NCB, %BWOC (Birla Carbon Egypt) | 0 | 0.05 | 0.1 | 0.2 |
| Distilled water, %BVOBF (ChemWorld) | 100 | 100 | 100 | 100 |

Table 5 Cement slurry compositions used in experiments based on API 10A

| Materials | C 5 | C 6 | C 7 | C 8 |
|------------------------------------|-----|------|-----|-----|
| Cement, %BWOC (Dyckerhoff) | 100 | 100 | 100 | 100 |
| NCB, %BWOC (Birla Carbon Egypt) | 0 | 0.05 | 0.1 | 0.2 |
| Distilled water, %BWOC (ChemWorld) | 44 | 44 | 44 | 44 |

high aspect ratios and excellent thermal and electrical conductivities. The physical and chemical characteristics of the nanocarbon black are presented in Table 3, in addition to the eight cement slurry compositions (C1, C2, C3, C4, C5, C6, C7, and C8) based on testing procedures

of API 10B-2 and API 10A standard guidelines used in this study are detailed in Tables 4 and 5. Conventional additives are used in cement systems to enhance specific properties. An antifoam chemical is added to prevent issues like gelation, cavitation, and reduced density caused by excessive foaming, by adjusting surface tension and improving the dispersion of solids, effectively eliminating foam formation (Nelson & Guillot, 2016). A fluid loss control agent such as an organic polymer is added to the slurry to prevent water loss in permeable zones. This avoids increased viscosity, annular bridge formation, and low-quality cement. Controlling fluid loss also prevents premature cement setting and formation damage (Bourgoyne, 1991; Cheung & Beirute, 1985). A cement extender is used to reduce slurry density to prevent lost circulation in weak formations and minimize well-completion stages. They also increase slurry yield by lowering the amount of cement required, enhancing cost-effectiveness in cementing. (Nelson & Guillot, 2016). A dispersant agent is added to the slurry to avoid viscosity fluctuation with temperature changes by maintaining workability during mixing and placement to ensure an even distribution of NCB particles for consistent cement paste (Y. Li et al., 2021). A retarder is added to cement slurries to extend the setting time and keep the cement pumpable for a longer duration before solidification (Schlumberger, 1984).

2.2 Cement Slurry Formulation

To facilitate result analysis and comparisons, cement slurry formulations are designed and conducted based on laboratory testing that replicates real field conditions such as bottom hole circulating temperature (BHCT: 190 °F), bottom hole static temperature (BHST: 237 °F), and bottom hole pressure (BHP: 6200 psi). Oil and gas well cement slurry formulations were prepared by following the API guidelines (API 10B-2, 2013) and (API 10A, 2019) to achieve a consistent specific density of 1.9 g/cm³ (15.8 lb/gal) and a water to cement (w/c) ratio of 44%. The NCB mixing ratios were kept at minimal concentrations of 0.05%, 0.1%, and 0.2% BWOC to prevent any negative effects from nanoparticle agglomeration in the cement slurry, as observed in previous studies with higher NCB concentrations. The NCBs were incorporated within four cement slurry compositions, including a neat cement formulation employed as a testing reference for comparison and evaluation to investigate the positive effects of NCB addition to the cement slurry properties in both liquid and solid states to get the optimal concentration of NCB at which the uniform dispersion of nanocarbon particles is ensured. Silica flour is added with a percentage of 35% BWOC into cement slurry to prevent cement sheath strength retrogression, which

occurs at an elevated bottomhole static temperature (BHST) above 230°F because some of the calcium silicate hydrate (C-S-H) gel combines with the calcium hydroxide (CH) to form alpha dicalcium silicate hydrate ($\alpha\text{C}_2\text{H}$), which usually results in shrinkage, decreases CS, and increases the permeability of the set cement (Young & Hansen, 1986). This phenomenon can be overcome by decreasing the overall lime-to-silicate ratio (C/S) ratio in the cement, preventing the conversion of C-S-H gel and CH to C_2SH (Yetunde & Ogbonna, 2011). Also, by introducing NCB with various concentrations into the cement system, we can enhance the CS and flexibility and reduce the permeability of the set cement sheath under HPHT conditions. Eight cement pastes with varying compositions were prepared and analyzed by laboratory experiments. The composition details of each paste and their corresponding designations will be used throughout this study.

2.3 Cement Slurry Preparation

The cement slurry compositions were prepared according to the guidelines recommended by (API 10B-2, 2013) and (API 10A, 2019), by applying the wet-mixing method for chemical additives and the dry-mixing method for blending the cement with silica flour, which is a widely employed approach for preparing oil well cement within the industry. Failure to follow the specified order of addition can cause unpredictable slurry behavior and negatively affect performance. So, it is recommended to follow the appropriate mixing order while preparing all compositions of cement slurries. The slurry mixing procedure involved first agitating distilled water at 4000 rpm, then sequentially adding the antifoam agent, fluid loss agent, extender, dispersant, and retarder. NCB was added and hydrated for 5 minutes at 4000 rpm to ensure uniform nanoparticle dispersion. Finally, add dry blended cementitious materials, and the agitation speed was increased to 12,000 rpm to achieve proper slurry mixing energy as per guidelines of API 10B-2, (2013). After slurry preparation, the cement paste is tested according to the two (API 10B-2 and 10A) standards referred to above to evaluate the effect of nanocarbon addition with various concentrations on slurry behavior under ideal conditions based on API 10A and actual simulated wellbore conditions based on API 10B-2.

2.4 Testing and Measurements

2.4.1 Slurry Density Measurements

The study involved measuring the density of the slurries right after the cement was mixed at atmospheric conditions according to the guidelines recommended by API 10B-2 (2013), using a standard pressurized mud



Fig. 3 Pressurized mud balance for slurry density measurements

balance as presented in Fig. 3. The recorded density values were in pounds per gallon (ppg) and were then compared to a reference slurry of pure cement.

2.4.2 Cement Slurry Rheology Measurements

The flow characteristics of the slurries were assessed by using a rotational viscometer (Chandler, Model 3500) as shown in Fig. 4, to confirm the impact of nanocarbon black on the workability of the fresh cement slurry at surface temperature 80°F and at bottomhole circulation temperature (BHCT) 190°F after conditioning the slurry on



Fig. 4 Rotational viscometer for slurry rheological parameters measurements

downhole conditions for 30 minutes in an atmospheric consistometer. The dial measurements were captured first in an increasing sequence and then in a decreasing sequence, using a maximum speed of 300 rpm. The ratio between the readings at each speed was employed to assess certain properties of the slurries. Gel strength, measured in lbf/100 ft², is an additional factor that can be extracted directly from the reading on the dial by allowing the sample to remain static for 10 s and then activating the viscometer at a typically low speed of 3 rpm. We then observe the highest point of deflection on the dial to be reported as 10 s gel strength and let the sample remain static for 10 min and record this value as the result of 10 minutes gel strength following the guidelines of (API 10B-2, 2013). Even though the Herschel–Bulkley rheological model is the most suitable way to depict the rheology of cement slurry, but Bingham model has been most widely used so that the rheological measurements of the slurries were documented as the mean of the two dial readings obtained at each speed to obtain the plastic viscosity and yield point of the slurry. It is recommended to perform a linear regression analysis using the complete set of available data points using Eq. (1):

$$\tau = \tau_y + [\mu_p \times \gamma] \quad (1)$$

where τ : shear stress, measured in Pa, or (lbf/100 ft²); τ_y : Bingham yield stress, measured in Pa, or (lbf/100 ft²); μ_p : plastic viscosity, measured in Pa·s, or (cP); γ : shear rate, measured in s⁻¹.

2.4.3 Cement Slurry Free Fluid Measurements

A free fluid test was conducted to assess the stability of the slurry to ensure that it can provide full zonal isolation and maintain the desired cement slurry properties. As evidenced in Fig. 5, the free fluid volume was determined by conditioning the slurry at 190°F, then pouring it into



Fig. 5 250-mL graduated cylinder for API 10B-2 slurry free fluid measurements

a graduated 250-mL plastic cylinder with a sealing cover and keeping it on an undisturbed (vibration-free) surface for 2 hours at 80°F according to guidelines listed in API 10B-2 (2013). We calculated the free fluid as a percentage of the volume of the slurry using Eq. (2). As illustrated in Figs. 6, 7, the free fluid test was performed according

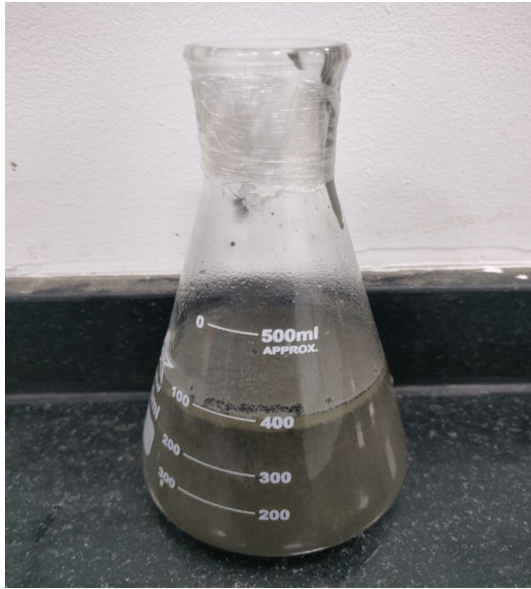


Fig. 6 500-mL conical flask for API 10A slurry free fluid measurements

to the recommended practice of API 10A (2019) by conditioning the slurry at 80°F for 20 min, then pouring 760 g of conditioned slurry into a 500-mL conical flask with a sealing cover and keeping it on an undisturbed (vibration-free) surface for 2 hours at 80°F. The free fluid (FF) percentage must not exceed 5.9% and can be calculated based on Eq. (3):

$$\varphi = \frac{V_{FF}}{V_s} \times 100 \tag{2}$$

$$\varphi = \left[\frac{(V_{FF} \times \rho_s)}{m_s} \right] \times 100 \tag{3}$$

where φ : slurry free fluid content percentage, measured in %; V_{FF} : volume of free fluid collected, measured in mL; V_s : initial volume of slurry, measured in mL; ρ_s : density of slurry, measured in g/cm^3 ; m_s : initial recorded mass of the slurry, measured in g.

2.4.4 Cement Slurry Sedimentation Measurements

When the cement slurry is left undisturbed for a certain duration, it can also undergo particle sedimentation. The settling process becomes evident through a density comparison of various sections within the solidified cement column (API 10B-2, 2013). The sedimentation of the cement sheath was assessed after conditioning the slurry in an atmospheric consistometer (Chandler, Model 1200) at 190°F for 30 min to simulate downhole placement



(a)



(b)

Fig. 7 a Sedimentation tube with 250-mm length, 25-mm inner diameter; b divided set cement column after curing for 24 h for sedimentation measurements

conditions. We then poured the conditioned slurry into a sedimentation tube that is 200 mm long and 25 mm in diameter. The tube is placed in a curing chamber in a vertical position for 24 hours at BHST (237°F) and testing pressure of 3000 psi until the conditioned slurry reached the set phase. We then removed the tube and allowed it to cool to 80°F using a water bath; after that, we measured and recorded the length of the specimen and the set cement drop, which is the gap separating the upper surface of the solidified cement from the upper surface of the initial slurry level. Next, cut 20 mm from each end of the set cement column and divide, then mark the set cement into at least four equal segments approximately 20 mm long. The segments were cut at marks while keeping their order and placed in water until ready to be weighed. The weight of each section was determined in both air and water to utilize Archimedes' principle for computing the relative density or specific gravity for each segment. Finally, the difference in density between the upper and lower portions of the solidified cement column was computed to indicate slurry sedimentation using Eq. (4):

$$\rho_{relative} = m_{air} / m_{water} \quad (4)$$

where $\rho_{relative}$: relative density of each set segment, dimensionless; m_{air} : mass of the cement segment in the air (dry mass), g; m_{water} : mass of the cement segment in the water (wet mass), g.

2.4.5 Cement Slurry Fluid Loss Measurements

The rate of fluid filtration rises as temperature increases, while pressure has a relatively minor impact on the filtration rate (Bourgoyne, 1991). Controlling the fluid loss (FL) of cement slurries is crucial for minimizing the drying out of the slurry within the porous sections of the well. As depicted in Fig. 8, the fluid loss filtrations of tested slurries across the permeable zones were measured by using a non-stirred fluid loss cell (Chandler, Model SFL387) at the bottomhole circulating temperature (190°F) and at an operating pressure of 1000 psi. Also, the filtrate volume is collected within 30 min. Furthermore, in the case of HPHT conditions as encountered in the wellbore, the filter paper should have half the surface area of the standard size. As a result, the measured filtrate volume needs to be multiplied by two before being recorded, as per standard guidelines (API 10B-2, 2013). The API fluid loss volume was calculated as described in Eq. (5):

$$V_{FL} = 2V_t \sqrt{(30/t)} \quad (5)$$

where V_{FL} : volume of fluid loss collected, measured in mL; V_t : filtrate volume collected within time (t), measured in mL; t : time, measured in minutes.



Fig. 8 Non-stirred fluid loss apparatus for slurry filtrate volume measurements

2.4.6 Cement Slurry Thickening Time Measurements

For the slurry thickening time (TT) test, an HPHT consistometer (Chandler, Model 8040) is used to determine the time it takes to thicken when tested with a specific schedule for a temperature and pressure to simulate the placement of slurry in the wellbore as demonstrated in Fig. 9. The consistometer typically includes a rotating cylindrical container for the slurry with a stationary paddle arrangement, all housed within a cylindrical pressure chamber that rotates at 150 rpm and is capable of enduring high pressures and temperatures. Initially, the slurry was exposed to a surface temperature (80°F) and atmospheric pressure during the batch mixing time for 2 hours, then raised to the bottomhole circulating temperature of 190°F and bottom hole pressure of 6200 psi within 2 hours, and then stabilized on these conditions until the end of the test as recommended practice (API 10B-2, 2013). Also, a thickening time test was performed for class-G cement slurry compositions based on API 10A (2019), in which the temperature and pressure are ramped from atmospheric conditions to 125°F and 5160 psi within 28 minutes and kept on these conditions until the end of the test. The slurry Bearden consistency (Bc) is characterized by the torque applied to the paddle due to the presence of the cement slurry that is measured over testing time to obtain the allowed thickening time for the slurry, which is recommended pumping time to avoid increasing in slurry viscosity and pumping pressure throughout the placement time of the cementing operation.



Fig. 9 HPHT consistometer for slurry thickening time measurements

2.4.7 Cement Slurry Compressive Strength Measurements

The CS of the slurry is analyzed by using the ultrasonic cement analyzer unit (Chandler, Model 4265) as observed from Fig. 10 for a nondestructive test with a curing period of 24 hours and load frame (Chandler, Model 4207D) and a curing chamber (Chandler, Model 7370) as indicated in Fig. 11 for a destructive crush test with a curing period of 7 days with the same pressure and temperature profile. The tests were performed by ramping to the BHST of the wellbore and to bottomhole pressure (BHP) within 4 hours, as per recommended procedures of API 10B-2 (2013), to evaluate the mechanical characteristics of cement sheath under harsh conditions

to replicate the actual stress experienced in the wellbore downhole conditions. Also, a CS test was performed for Class-G cement slurry compositions based on API 10A (2019), which cured at a temperature of 100°F for 8 hours. The minimum strength achieved after the curing period varies based on the type of cement used and the curing conditions. We calculated the CS by dividing the force needed to fracture the specimen with the smallest cross-sectional area touching the load-bearing plates of the load frame using Eq. (6):

$$CS = F_{max} / A_{min} \tag{6}$$



Fig. 10 Ultrasonic cement analyzer for nondestructive CS measurements



Fig. 11 Load frame for destructive CS measurements

where CS: compressive strength of the sample, measured in psi; F_{max} : maximum force attained prior to failure, measured in lbf; A_{min} : minimum cross-sectional area of the sample, measured in in.²

2.4.8 Cement Slurry Tensile Strength measurements

Indirect tensile strength, which is referred to as the splitting tensile strength or the Brazilian tensile strength, can be used to determine tensile strength. Similar to the CS test, all slurry specimens undergo the same curing conditions for 7 days. The test involves applying compressive force

across the diameter of the cylindrical cement sample until it fails as seen in Fig. 12. It is crucial to ensure that the failure crack occurs in the same direction as the applied load to obtain an accurate result (Iremonger et al., 2015). The splitting tensile strength was calculated as described in Eq. (7):

$$\sigma_T = \frac{2F}{\pi hD} \quad (7)$$

where σ_T : tensile strength of specimen, measured in psi; F : axial compressive failure load, measured in lbf; h : height of specimen, measured in in.; D : diameter of specimen, measured in in.

2.4.9 Cement Sheath Porosity Measurements

In this study, we used the helium porosimeter as shown in Fig. 13 to determine the grain volume, pore volume, and porosity percentage for all hardened specimens with 1.5-in diameter and 2.7-in length, via an isothermal helium expansion into the chamber from a reservoir of known volume and pressure until equilibrium pressure is reached (20 to 60 min). The grain volume can be calculated by measuring the new gas pressure by applying Boyle's law, and the grain volume of the specimen is calculated mathematically using Eq. (8). The effective porosity is calculated by taking the difference of the bulk volume and grain volume using Eq. (9) (Luffel & Howard, 1988):

$$P_r V_r = P_2 (V_r + V_s - V_g) \text{ or } P_1 V_2 = P_2 V_2 \quad (8)$$

$$\phi = \left[\frac{(V_b - V_g)}{V_b} \right] \times 100 \quad (9)$$



Fig. 12 Splitting tensile strength (Brazilian test) for cement sheath compositions **a** before applying axial compressive failure load; **b** after applying axial compressive failure load



Fig. 13 Porosity test for cement sheath compositions after curing for 7 days at downhole conditions

where ϕ porosity of the sample, measured in %; V_b : bulk volume of the sample, measured in cm^3 ; V_g : grain volume of the sample, measured in cm^3 ; L : length of the sample, measured in mm;

D : diameter of the sample, measured in mm.

2.4.10 Cement Sheath Permeability Measurements

The permeability of a porous medium refers to its capacity to permit fluid to flow through it (Alkhamis & Imqam, 2018). High permeability is undesirable, as it deteriorates the cement sheath zonal isolation. Hence, it is essential to minimize the permeability of the cement sheath as much as possible. The API 10B-2 standard provides a procedural guideline for measuring the relative permeability of cured cement to liquids or gases (Nelson & Guillot, 2016). To measure gas permeability, it is necessary to dry the sample, which can be achieved by placing it over a desiccant or using a vacuum oven or a high-temperature oven (Mindess et al., 1981). As reflected in Fig. 14, the gas permeability of the cured cement is determined by introducing fluid into the core at a constant pressure difference along its length. The gas permeability of the cured cement sample can be calculated using Darcy's law, as in Eq. (10):

$$k = \left[\frac{(2000 \times \mu_{gas} \times q_{gas} \times p \times L)}{A \times [(p_{inlet})^2 - (p_{outlet})^2]} \right] \quad (10)$$

where k : permeability to gas, measured in mD; q_{gas} : flow rate of gas, measured in mL/s; μ_{gas} : viscosity of the gas, measured in cP; L : length of the sample, measured in cm; A : sample cross-sectional area, measured in cm^2 ; p : adjusted barometric pressure, measured in atm; p_{inlet} : inlet gas pressure, measured in atm; p_{outlet} : outlet gas pressure, measured in atm.

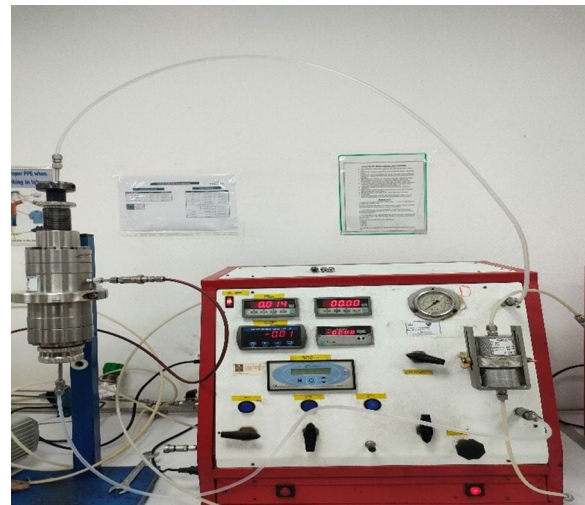


Fig. 14 Permeability test for cement sheath compositions after curing for 7 days at downhole conditions

3 Results and Discussion

3.1 Cement Slurry Density

The initial density of the pure cement system was approximately 15.8 ppg, as observed in Fig. 15. With the addition of 0.05%, 0.1%, and 0.2% NCB BWOC, the density increased slightly by 0.06%, 0.13%, and 0.25%, respectively. These minor increases can improve the cement sheath integrity, which is beneficial for primary and remedial wellbore cementing applications like plugs, squeezes, and casing cementing operations. Mean density values for all analyzed slurries in this study are provided in Table 6.

3.2 Cement Slurry Rheological Behavior

The rheological flow curves for the four cement designs were nearly identical, forming straight lines at both surface and downhole temperatures, indicating minimal impact from NCB on rheological behavior. At surface

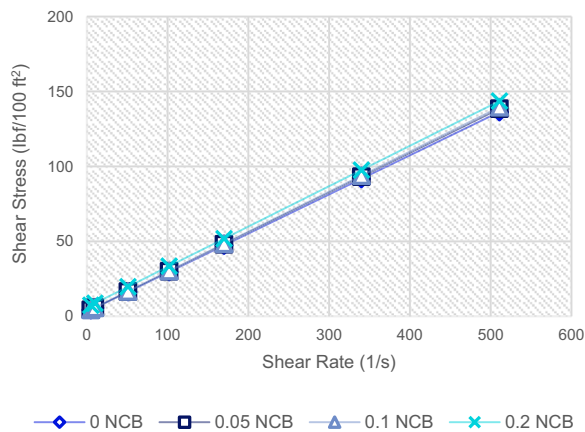


Fig. 16 Rheological behavior of various slurry compositions at surface temperature

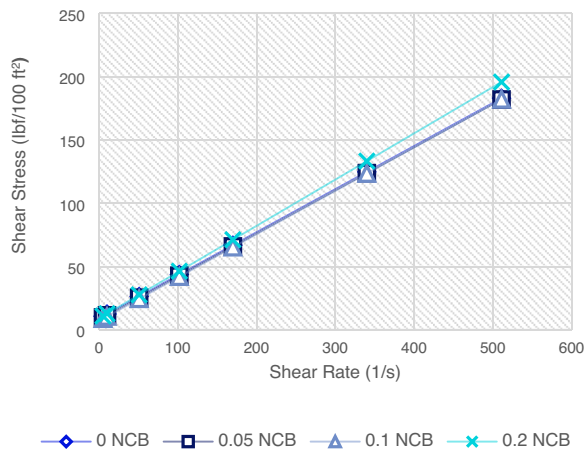


Fig. 17 Rheological behavior of various slurry compositions at downhole temperature

3.3 Cement Slurry Free Fluid

The results indicate that NCB acts as a bridging agent, filling gaps between cement particles and reducing the mobility of free fluids. This reduction in free fluid content helps maintain the cement’s effective density, lowering hydrostatic pressure and preventing the formation of channels within the cement barrier, as observed in previous studies (Webster & Eikerts, 1979).

3.3.1 Free Fluid Testing Based on the Specification of API 10B-2

The inclusion of NCB significantly reduced free fluid volume in the cement system. The addition of 0.05% NCB BWOC led to a 25% reduction, while 0.1% NCB BWOC resulted in a 50% reduction in free fluids within the cement slurry, as detailed in Table 9.

Table 9 Free fluid volume percentage for API 10A and API 10B-2 cement slurry compositions

| Cement slurry compositions | Free fluid% [API 10A] | Free fluid% [API 10B-2] |
|--|-----------------------|-------------------------|
| C1 (neat slurry system) | 2.52 | 0.04 (trace) |
| C2 (neat slurry system + 0.05% NCB BWOC) | 2.44 | 0.03 (trace) |
| C3 (neat slurry system + 0.1% NCB BWOC) | 2.28 | 0.02 (trace) |
| C4 (neat slurry system + 0.2% NCB BWOC) | 3.00 | 0.12 (trace) |

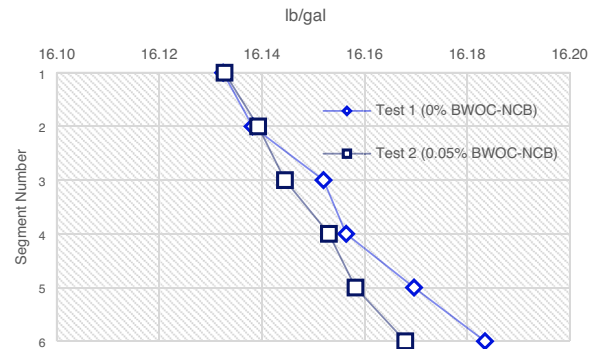


Fig. 18 Sedimentation curves after 24-h curing for 0% and 0.05% BWOC NCB slurries

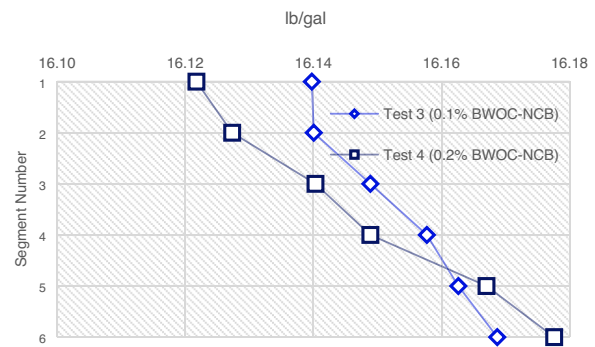


Fig. 19 Sedimentation curves after 24-h curing for 0.1% and 0.2% BWOC NCB slurries

3.3.2 Free Fluid Testing Based on the Specification of API 10A

According to API 10A specifications, the addition of NCB had a slight impact on free fluid content. At concentrations of 0.05% and 0.1% BWOC, NCB reduced free fluids in the cement slurry by 3.17% and 9.52%, respectively. These findings are represented in Table 9 for clarity.

3.4 Cement Slurry Sedimentation

Figs. 18 and 19 show that all cement systems demonstrated strong stability, with no significant sedimentation observed. The incorporation of NCB

Table 10 Sedimentation for API 10B-2 cement slurry compositions

| Cement slurry compositions | Downgrade [mm] | Δ SG [g/cm ³] |
|--|----------------|---------------------------|
| C1 (neat slurry system) | 0.40 | 0.0060 |
| C2 (neat slurry system + 0.05% NCB BWOC) | 0.20 | 0.0048 |
| C3 (neat slurry system + 0.1% NCB BWOC) | 0.10 | 0.0036 |
| C4 (neat slurry system + 0.2% NCB BWOC) | 0.50 | 0.0072 |
| (API 10B-2 standard limits) | ≤ 5.00 | ≤ 0.06 |

Table 11 Fluid loss filtrate volume for API 10B-2 cement slurry compositions

| Cement slurry compositions | API fluid loss [mL] |
|--|---------------------|
| C1 (neat slurry system) | 53.00 |
| C2 (neat slurry system + 0.05% NCB BWOC) | 52.00 |
| C3 (neat slurry system + 0.1% NCB BWOC) | 50.00 |
| C4 (neat slurry system + 0.2% NCB BWOC) | 55.00 |

did not negatively affect the cement’s characteristics. Stability, indicated by the absence of free fluids and noticeable settling (Al-Yami et al., 2010), was maintained across all tested samples. Detailed sedimentation test data are available in Table 10.

3.5 Cement Slurry Fluid Loss

The results depicted in Table 11 show that NCB acts as a bridging agent, filling gaps between cement particles and reducing fluid loss in the well formation. This reduction preserves the cement system’s integrity. Specifically, the inclusion of 0.05% and 0.1% NCB BWOC resulted in fluid loss reductions of approximately 1.88% and 5.66%, respectively.

3.6 Cement Slurry Thickening Time

3.6.1 Thickening Time Testing Based on the Specification of API 10B-2

The addition of NCB to the cement slurry system reduces the time needed for the cement slurry to thicken, as demonstrated in Figs. 20 and 21. According to the specification of API 10B-2, the experimental data reveal that the addition of nanomaterials at concentrations of 0.05%, 0.1%, and 0.2% BWOC of NCB resulted in a decrease in thickening time by approximately 4.32%, 5.15%, and 1.99%, respectively. The potential for premature setting of the NCB slurry system can be adjusted by using an appropriate concentration of retarder to meet the thickening time requirements for wellbore cementing applications. These outcomes are summarized in Table 12.

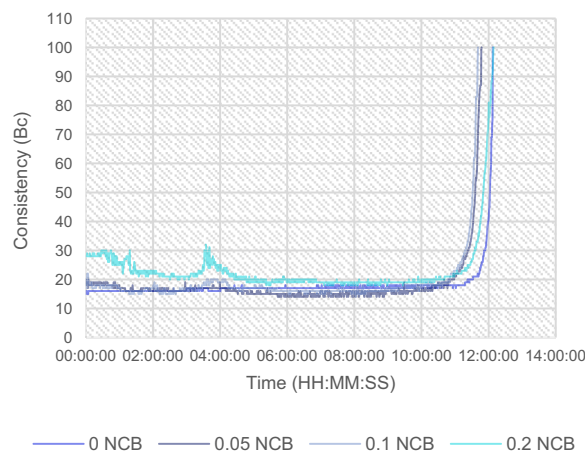


Fig. 20 Thickening time curves for API 10B-2 cement slurry compositions

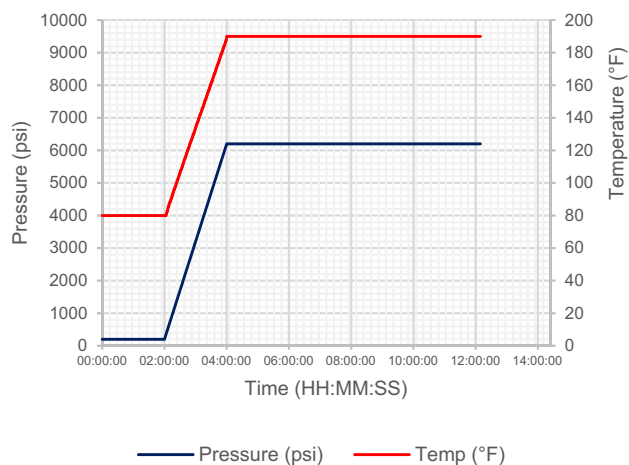


Fig. 21 API 10B-2 pressure and temperature profiles during the thickening time test

3.6.2 Thickening Time Testing Based on the Specification of API 10A

Figs. 22 and 23 show that adding NCB to the cement system according to API 10A reduces the thickening

Table 12 Thickening time for API 10A and API 10B-2 cement slurry compositions

| Cement slurry compositions | Time to 100 Bc [API 10A] [hr:mn] | Time to 50 Bc [API 10B-2] [hr:mn] |
|---|----------------------------------|-----------------------------------|
| C1 (neat slurry system) | 1:58 | 10:02 |
| C2 (neat slurry system + 0.05%NCB bwoc) | 1:56 | 09:36 |
| C3 (neat slurry system + 0.1%NCB bwoc) | 1:53 | 09:31 |
| C4 (neat slurry system + 0.2%NCB bwoc) | 1:57 | 09:50 |

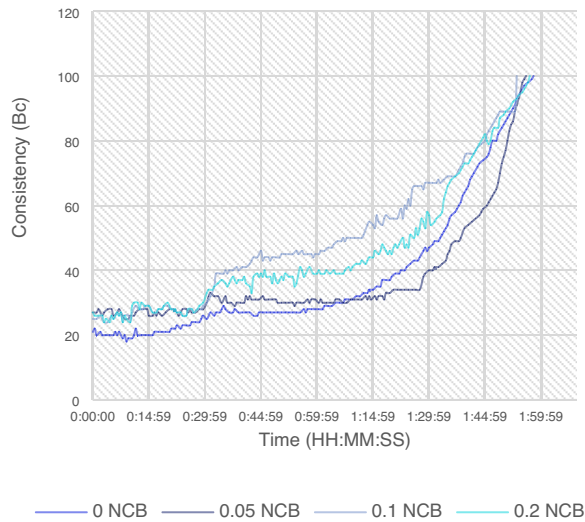


Fig. 22 Thickening time curves for API 10A cement slurry compositions

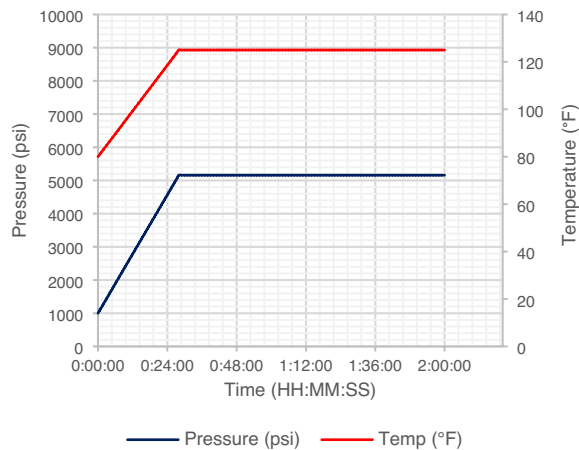


Fig. 23 API 10A pressure and temperature profiles during the thickening time test

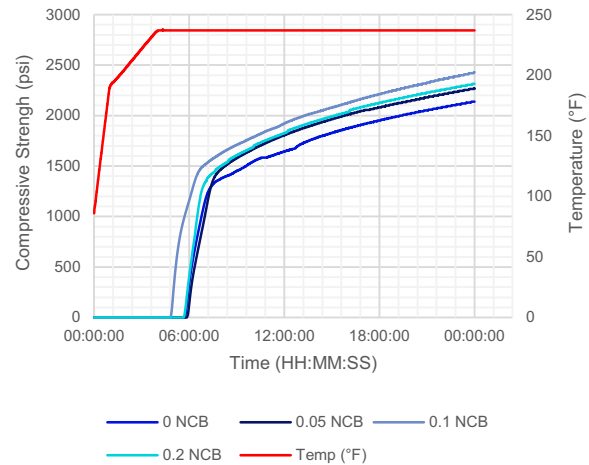


Fig. 24 Compressive strength curves during 24 h for API 10B-2 cement slurry compositions

time of the slurry. Specifically, 0.05%, 0.1%, and 0.2% NCB BWOC decreased thickening time by approximately 1.69%, 4.24%, and 0.85%, respectively. Detailed results are summarized in Table 12.

3.7 Cement Sheath Compressive Strength

3.7.1 Compressive Strength Based on the Specification of API 10B-2

The addition of NCB to the cement system significantly enhanced the compressive strength of the cement sheath. Experimental data showed that incorporating 0.05% NCB BWOC resulted in a noticeable strength increase. Notably, when incorporating 0.1% BWOC of NCB, it resulted in an early compressive strength (50 psi) that indicated the addition of NCB facilitated acceleration of cement slurry chemical hydration reactions, which contributed to reducing wait-on-cement time. Strength gains of 13.66% and 12.35% were observed, respectively, after the slurry was cured under simulated wellbore downhole conditions for 1 day in an ultrasonic cement

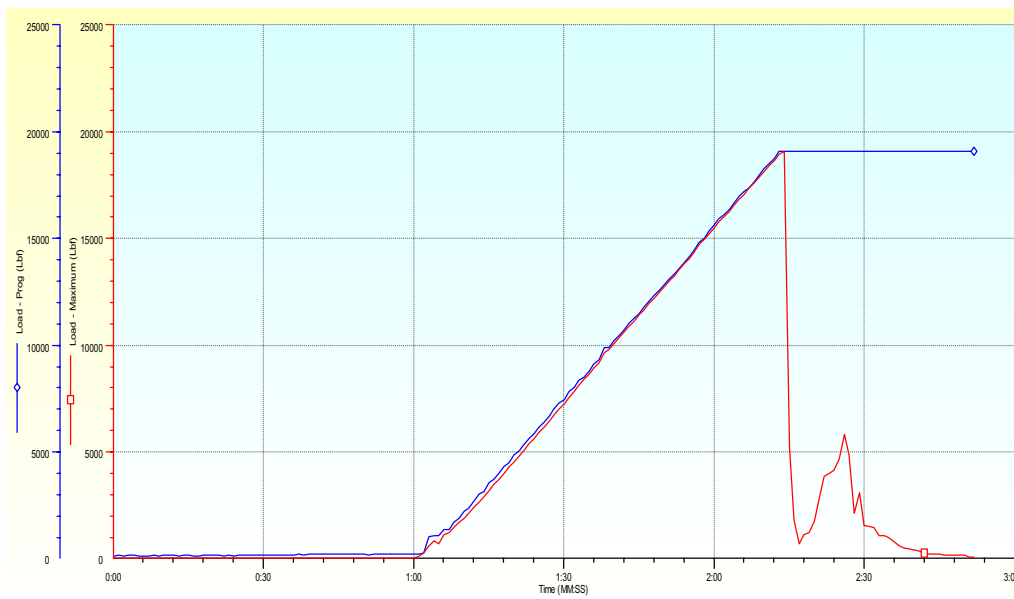


Fig. 25 Compressive strength curve for API 10B-2 for 0% BWOC NCB slurry after 7 days of curing at downhole conditions

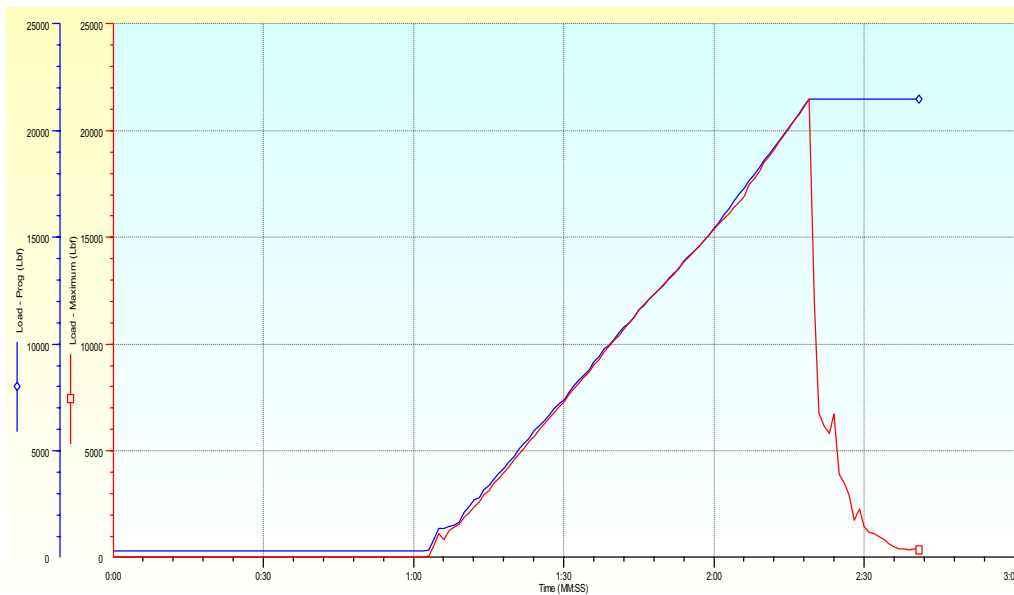


Fig. 26 Compressive strength curve for API 10B-2 for 0.05% BWOC NCB slurry after 7 days of curing at downhole conditions

analyzer (UCA) and for 7 days in a curing chamber for a compressive strength test, as illustrated in Figs. 24, 25, 26, 27, and 28. Detailed improvements in compressive strength measurements are provided in Table 13 for reference.

3.7.2 Compressive Strength Based on the Specification of API 10A

According to API 10A guidelines for slurry compressive strength testing at 100°F, adding NCB to the cement system significantly improved compressive strength. Incorporating 0.05%, 0.1%, and 0.2% NCB BWOC increased approximately 8.15%, 10.09%, and 8.70%,

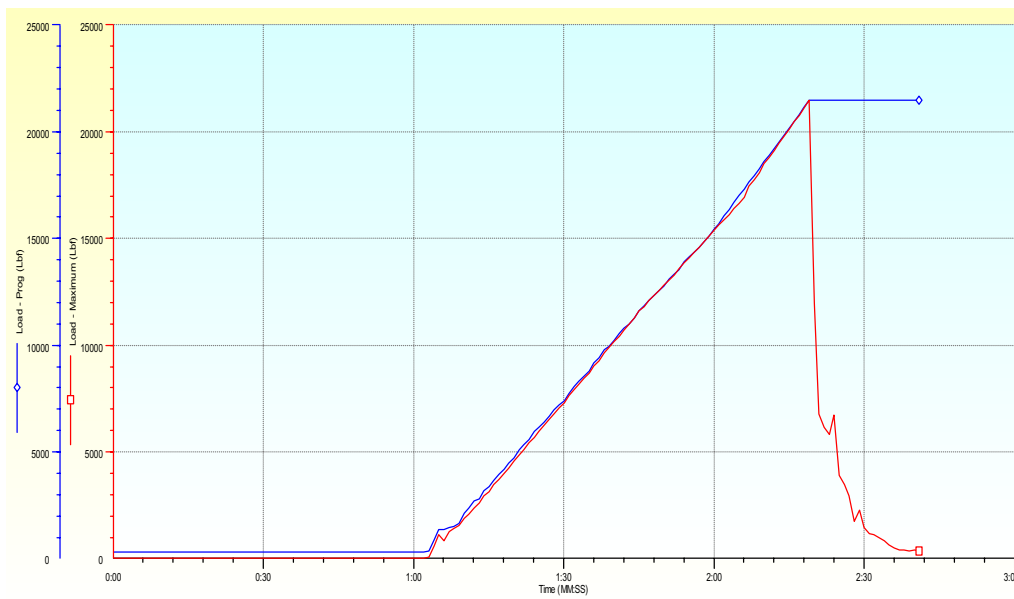


Fig. 27 Compressive strength curve for API 10B-2 for 0.1% BWOC NCB slurry after 7 days of curing at downhole conditions

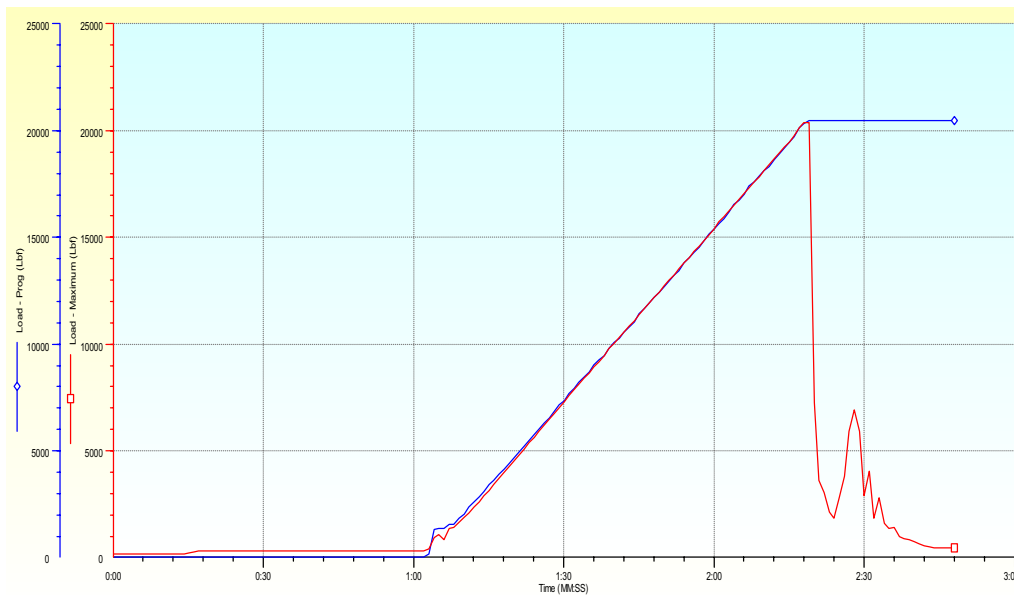


Fig. 28 Compressive strength curve for API 10B-2 for 0.2% BWOC NCB slurry after 7 days of curing at downhole conditions

respectively. Detailed improvements are shown in Figs. 29, 30, 31, and 32 and summarized in Table 13.

3.8 Cement Sheath Tensile Strength

Fig. 12 depicts the use of splitting tensile strength (Brazilian test) for cement sheath. The experimental results show that adding NCBs significantly improved the tensile strength of cement systems, which is beneficial for oil well applications. With NCB concentrations of 0.05%, 0.1%, and 0.2% BWOC, tensile

Table 13 Compressive strength and average load for API 10A and API 10B-2 cement slurry compositions

| Cement slurry compositions | Compressive strength [psi] Average load (lbf) | | |
|----------------------------|---|--------------------------------------|---|
| | Crush test API 10A 8 h [CS-psi] (Avg load-lbf) | UCA API 10B-2 24 h [CS-psi] | Crush test API 10B-2 7 days [CS-psi] (Avg load-lbf) |
| C1 | [1080] (4258) | [2138] | [4694] (19060) |
| C2 | [1168] (4592) | [2268] | [4955] (20021) |
| C3 | [1189] (4712) | [2430] | [5274] (21416) |
| C4 | [1174] (4603) | [2315] | [5010] (20445) |

Conversion factor: 1 psi = 6894.7572 Pa

strength increased by 14.43%, 77.46%, and 36.57%, respectively, compared to the reference system. The detailed results are provided in Table 14.

3.9 Cement Sheath Porosity

Fig. 13 depicts the use of a helium porosimeter to assess the influence of NCB inclusion in the cement system. Experimental results show that adding NCB to the cement system significantly reduced porosity. Specifically, concentrations of 0.1% and 0.2% NCB BWOC decreased porosity by about 21.04% and 22.56%, respectively, compared to the reference system. These findings are summarized in Table 15.

3.9.1 Cement Sheath Permeability

Fig. 14 depicts the use of a nitrogen gas permeameter and all instruments needed for specimen preparation. Experimental results show that incorporating NCB into the cement system effectively reduces permeability without adverse effects. Specifically, NCB concentrations of 0.05%, 0.1%, and 0.2% BWOC decreased permeability by approximately 13.53%, 19.05%, and 19.32%, respectively, compared to the reference system. These findings are detailed in Table 16.

Study's Limitations: At high concentrations of NCBs, nanoparticles were poorly dispersed due to nanofiller agglomeration and increased size of NCB aggregates (Hawreen et al., 2018), which led to adverse effects on the slurry density, flow characteristics, and thickening time required for cementing operations.

4 Conclusions

Following the standard guidelines set by API 10A and API 10B-2, this study systematically evaluated the effects of incorporating NCBs into Class-G Portland cement at concentrations ranging from 0.05% to 0.2% BWOC. The key findings from these extensive assessments are summarized as follows:

1. The addition of minimal concentrations of NCBs (0.05%, 0.1%, and 0.2% BWOC) resulted in slight

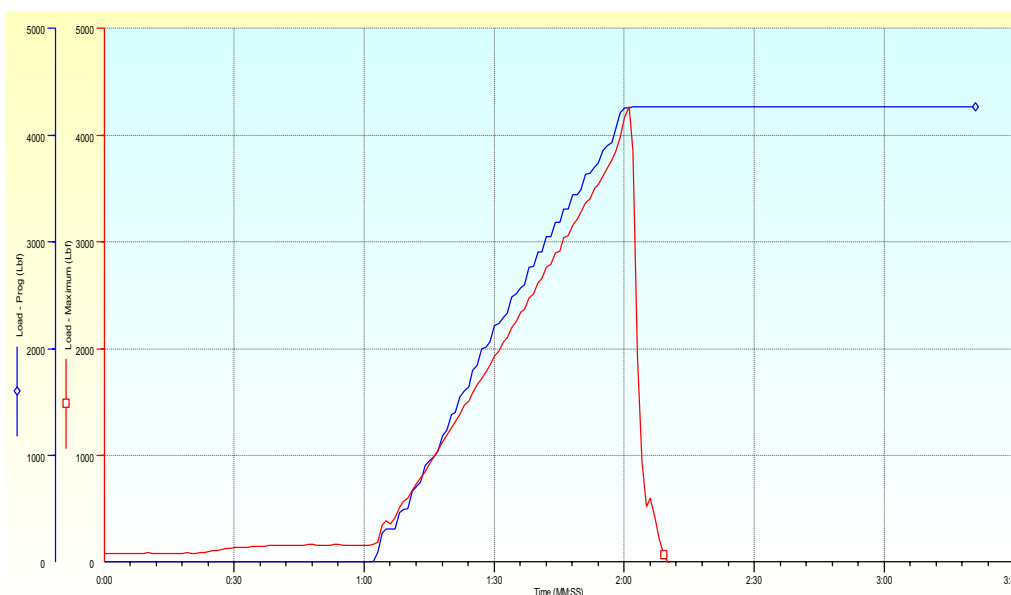


Fig. 29 Compressive strength curve for API 10A for 0% BWOC NCB slurry after 8 h of curing at 100°F

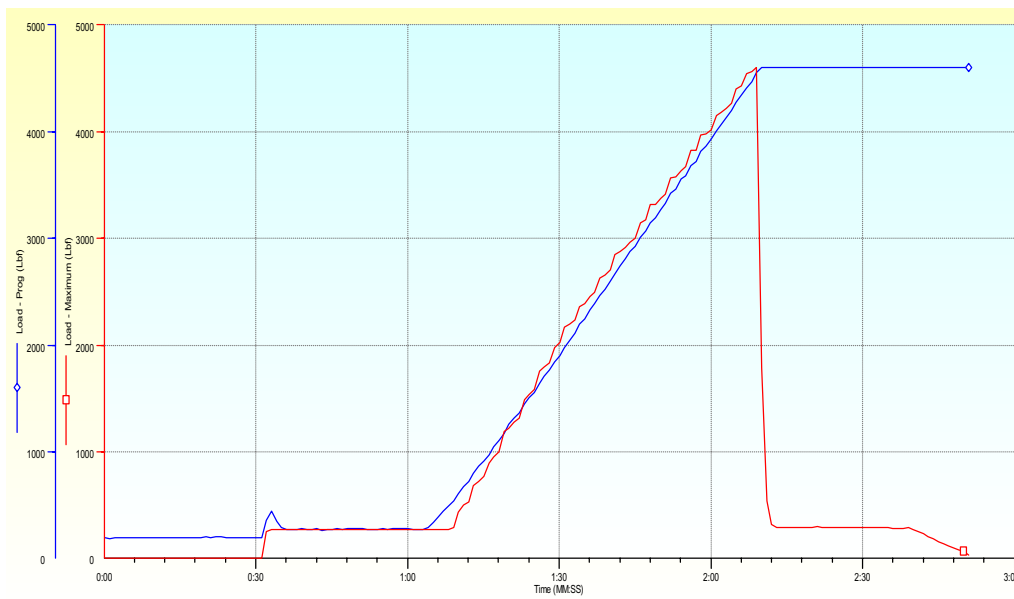


Fig. 30 Compressive strength curve for API 10A for 0.05% BWOC NCB slurry after 8 h of curing at 100°F

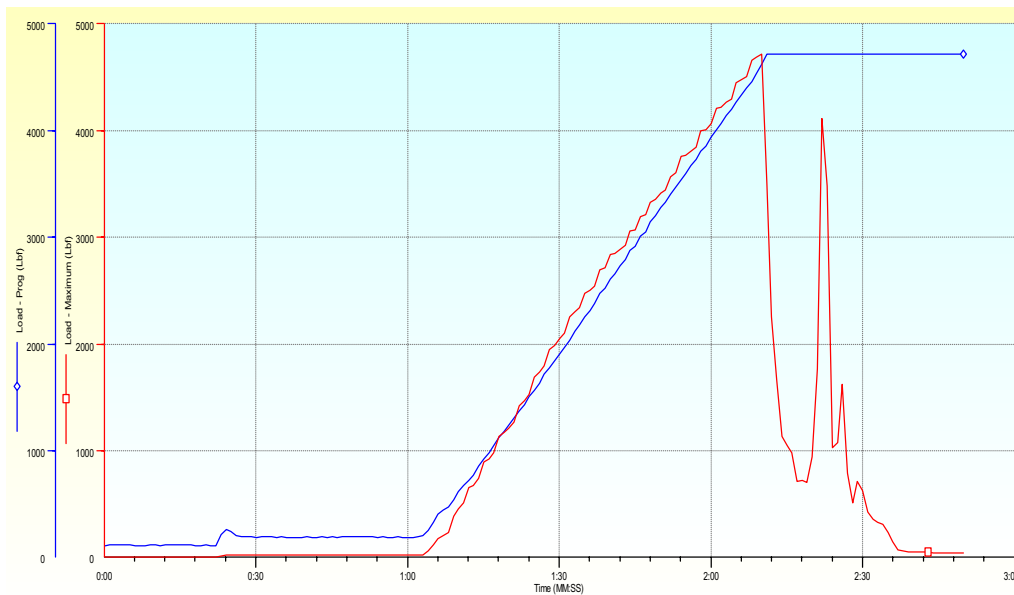


Fig. 31 Compressive strength curve for API 10A for 0.1% BWOC NCB slurry after 8 h of curing at 100°F

density increases of 0.06%, 0.13%, and 0.25%, respectively. These increases proved beneficial for wellbore cementing applications, enhancing the overall performance and integrity of the cement system.

2. The addition of NCB had minimal impact on the rheological behavior of the cement, as flow curves remained nearly identical across different tem-

peratures. At surface temperature, plastic viscosity increased and yield stress doubled with 0.2% NCB. At downhole temperatures, yield stress decreased by 11.11% and 22.22% with 0.05% and 0.1% NCB, respectively.

3. Incorporating NCBs into cement systems improved stability and reduced free fluid content, with

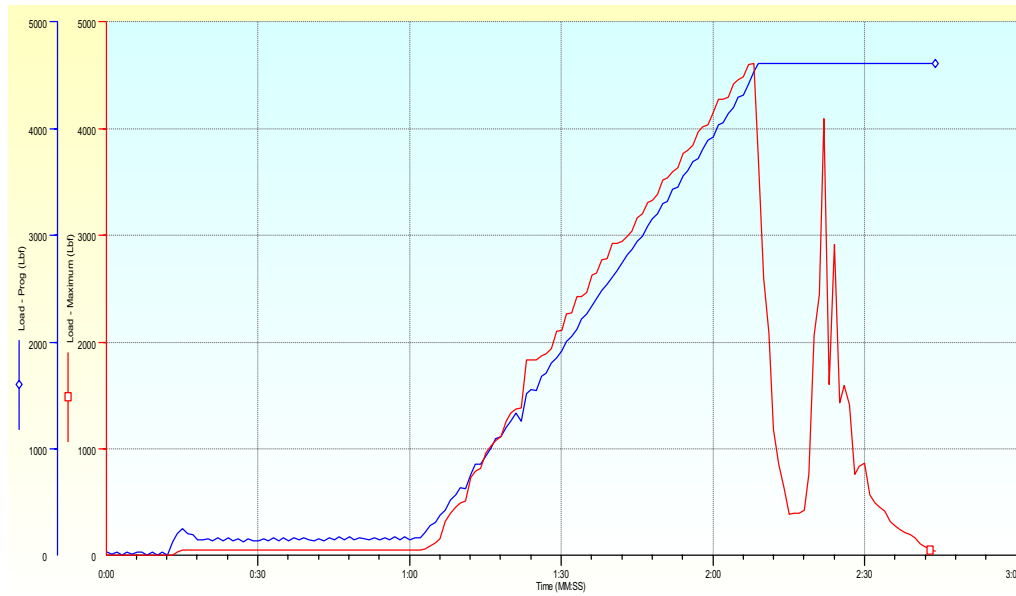


Fig. 32 Compressive strength curve for API 10A for 0.2% BWOC NCB slurry after 8 h curing at 100°F

Table 14 Splitting tensile strength (Brazilian test) for cement slurry compositions

| Tensile strength [psi] Cement slurry compositions | [7 days] |
|---|----------|
| C1 (neat slurry system) | 202.84 |
| C2 (neat slurry system + 0.05%NCB BWOC) | 232.12 |
| C3 (neat slurry system + 0.1%NCB BWOC) | 359.95 |
| C4 (neat slurry system + 0.2%NCB BWOC) | 277.02 |

Table 15 Porosity for cement slurry compositions after curing for 7 days at downhole conditions

| Porosity [%] Cement slurry compositions | [7 days] |
|---|----------|
| C1 (neat slurry system) | 24.29 |
| C2 (neat slurry system + 0.05%NCB BWOC) | 21.09 |
| C3 (neat slurry system + 0.1%NCB BWOC) | 19.18 |
| C4 (neat slurry system + 0.2%NCB BWOC) | 18.81 |

reductions of 3.17% and 9.52% at 0.05% and 0.1% BWOC per API 10A, and 25% and 50% per API 10B-2. This enhancement is due to the larger surface area of NCB particles, with no significant sedimentation observed.

4. NCB acts as a bridging agent, reducing fluid loss in the well formation and preserving cement integrity.

Table 16 Permeability for cement slurry compositions after curing for 7 days at downhole conditions

| Permeability [mD] Cement slurry compositions | [7 days] |
|--|----------|
| C1 (neat slurry system) | 0.1181 |
| C2 (neat slurry system + 0.05%NCB BWOC) | 0.1022 |
| C3 (neat slurry system + 0.1%NCB BWOC) | 0.0956 |
| C4 (neat slurry system + 0.2%NCB BWOC) | 0.0953 |

Conversion factor: 1 mD = 9.869233e-16 m²

Incorporating 0.05% and 0.1% NCB BWOC reduced fluid loss by approximately 1.88% and 5.66%, respectively.

5. Adding NCB to the cement system reduced the thickening time by 1.69%, 4.24%, and 0.85% per API 10A and by 4.32%, 5.15%, and 1.99% per API 10B-2, at 0.05%, 0.1%, and 0.2% BWOC, respectively, due to accelerated chemical hydration reactions of slurries. However, at higher NCB concentrations, agglomeration occurs, necessitating an increase in dispersant or retarder to maintain proper slurry dispersion and meet cementing operation requirements.

5 Future work

1. Optimizing the concentration and dispersion of nano-carbon black particles for specific oil well cementation applications.
2. Using seawater in replacement of fresh water as base mix water for cement slurry compositions to ensure the stability, consistency, and mechanical characteristics of the cement slurry to be applicable for offshore cementing operations.
3. Testing the static gel strength by utilizing a static gel strength analyzer (SGSA) to check the occurring probabilities of gas migration throughout the cement slurry column in the transition phase.

Acknowledgements

The authors would like to thank SLB for their support in providing materials in cooperation with Birla Carbon Inc., and permission to publish this laboratory study. Also, the authors are grateful for the necessary support provided by laboratories of Cairo University, American University in Cairo, and Corex.

Author contributions

AE contributed to the conception, experimental investigation, resources, and writing—original draft; HK and SF were involved in formal analysis, methodology, supervision, validation, and writing, reviewing and editing. All the authors read and approved the final manuscript.

Funding

Open access funding provided by The Science, Technology & Innovation Funding Authority (STDF) in cooperation with The Egyptian Knowledge Bank (EKB).

Availability of data and materials

The datasets used or analyzed during the current study are available from the corresponding author on reasonable request.

Declarations

Consent for publication

All the authors agree that the article will be published after acceptance.

Competing interests

The authors declare that they have no competing interests.

Received: 15 June 2024 Accepted: 3 November 2024

Published: 5 February 2025

References

- Alkhamis, M., and Imqam, A. (2018). New Cement Formulations Utilizing Graphene Nano Platelets to Improve Cement Properties and Long-term Reliability in Oil Wells. In Society of Petroleum Engineers - SPE Kingdom of Saudi Arabia Annual Technical Symposium and Exhibition 2018, SATS 2018. <https://doi.org/10.2118/192342-ms>
- Al-Yami, A. S., Nasr-El-Din, H. A., Al-Humaidl, A. S., Al-Saleh, S. H., & Al-Arfaj, M. K. (2010). Evaluation and optimization of low-density cement: laboratory studies and field application. *SPE Drilling Completion*, 25(1), 70–89. <https://doi.org/10.2118/113090-PA>
- API 10A. (2019). Cements and Materials for Well Cementing. March. API 10B-2. (2013). 10B-2 Recommended Practice for Testing Well Cements., 124.
- Bourgoyne, A. T. (1991). *Applied drilling engineering*. Richardson TX: Society of Petroleum Engineers.
- Cheung, P. S. R., & Beirute, R. M. (1985). Gas flow in cements. *JPT, J Petrol Technol*, 37(7), 1041–1048. <https://doi.org/10.2118/11207-pa>
- De La Roi, R., Egyed, C., & Lips, J. P. (2012). Nano-engineered oil well cement improves flexibility and increases compressive strength: a laboratory study. *Soc Petrol Eng SPE Int Oilfield Nanotechnol Conf*, 2012, 157–167. <https://doi.org/10.2118/156501-ms>
- Deshpande, A., and Patil, R. (2017). *Applications of Nanotechnology in Oilwell Cementing*. SPE-183727-MS.
- De Souza, T. C., Pinto, G., Cruz, V. S., Moura, M., Ladeira, L. O., & Calixto, J. M. (2020). Evaluation of the rheological behavior, hydration process, and mechanical strength of Portland cement pastes produced with carbon nanotubes synthesized directly on clinker. *Const Build Mater*, 248, 118686. <https://doi.org/10.1016/j.conbuildmat.2020.118686>
- Fakher S. et al., 2023q. Development and optimization of epoxy-resin based cement reinforced with low-cost fly ash for high durability environmentally friendly cement. Paper presented at the 57th U.S. Rock Mechanics/Geomechanics Symposium, Atlanta, Georgia, USA, June 2023. <https://doi.org/10.56952/ARMA-2023-0197>.
- Fakher S. et al., 2023b. Direct carbon dioxide capture at atmospheric conditions via adsorption desorption hysteresis using shape-dependent pozzolanic material. Paper presented at the 57th U.S. Rock Mechanics/Geomechanics Symposium, Atlanta, Georgia, USA, June 2023. <https://doi.org/10.56952/ARMA-2023-0199>.
- Fakher, S., & Khlaifat, A. (2023). Experimental investigation of polymer injection in high permeability conduits for material sustainability and behavior in oil reservoirs. *Polymers*, 15(13), 2950. <https://doi.org/10.3390/polym15132950>
- Helmy, Y., & Fakher, S. (2024). Evaluating the performance of class F Fly Ash compared to class G cement for hydrocarbon wells cementing: an experimental investigation. *Materials*, 17(11), 2710. <https://doi.org/10.3390/ma17112710>
- Iremonger, S. S., Bolt, M., & Lawrence, S. C. (2015). Enhanced thermal well integrity through the use of a new cement tensile strength-enhancing fiber. *Soc Petrol Eng SPE Can Heavy Oil Techn Conf 2015 CHOC*. <https://doi.org/10.2118/174483-ms>
- Jafariefad, N., Geiker, M. R., Gong, Y., Skalle, P., Zhang, Z., & He, J. (2017). Cement sheath modification using nanomaterials for long-term zonal isolation of oil wells: review. *J Petrol Sci Eng*. <https://doi.org/10.1016/j.petrol.2017.06.047>
- Jimenez, W. C., Urdaneta, J. A., Pang, X., Garzon, J. R., Nucci, G., & Arias, H. (2016). Innovation of annular sealants during the past decades and their direct relationship with on/offshore wellbore economics. *SPE Bergen One Day Seminar*. <https://doi.org/10.2118/180041-MS>
- Khlaifat, A., et al. (2024). Evaluating factors impacting polymer flooding in hydrocarbon reservoirs: laboratory and field-scale applications. *Polymers*, 16(1), 75. <https://doi.org/10.3390/polym16010075>
- Li, G. Y., Wang, P. M., & Zhao, X. (2005). Mechanical behavior and microstructure of cement composites incorporating surface-treated multi-walled carbon nanotubes. *Carbon*, 43(6), 1239–1245. <https://doi.org/10.1016/j.carbon.2004.12.017>
- Li, Y., Dong, S., Ahmed, R., Zhang, L., & Han, B. (2021). Improving the mechanical characteristics of well cement using botryoid hybrid nano-carbon materials with proper dispersion. *Const Build Mater*. <https://doi.org/10.1016/j.conbuildmat.2020.121464>
- Luffel, D. L., & Howard, W. E. (1988). Reliability of laboratory measurement of porosity in tight gas sands. *SPE Form Eval*. <https://doi.org/10.2118/16401-pa>
- Mindess, S., Young, J. F., & Darwin, D. (1981). Concrete, prentice-hall. *Englewood Cliffs, NJ*, 481, 86–87.
- Nelson E, Guillot D. (2016). *Well Cementing* (E. Nelson and D. Guillot (eds.); Second Ed).
- Nochayia, T., & Chaipanich, A. (2011). Behavior of multi-walled carbon nanotubes on the porosity and microstructure of cement-based materials. *Appl Surface Sci*, 257(6), 1941–1945. <https://doi.org/10.1016/j.apsusc.2010.09.030>
- Nunes, J., Paula, D., Márcio, J., Orlando, L., Ludvig, P., Cruz, T., Souza, C., Marcelo, J., Vargas, A. A., & Melo, D. (2014). Mechanical and rheological behavior of oil-well cement slurries produced with clinker containing carbon nanotubes. *J Petrol Sci Eng*. <https://doi.org/10.1016/j.petrol.2014.07.020>

- Peyvandi, A., Taleghani, A. D., Soroushian, P., & Cammarata, R. (2017). The use of low-cost graphite nanomaterials to enhance zonal isolation in oil and gas wells. In *SPE Ann Techn Conf Exhib*. <https://doi.org/10.2118/187105-MS>
- Rezania, M., Panahandeh, M., Razavi, S. M. J., & Berto, F. (2019). Experimental study of the simultaneous effect of nano-silica and nano-carbon black on permeability and mechanical properties of the concrete. *Theoretical Appl Fract Mecha*, 104, 102391. <https://doi.org/10.1016/j.tafmec.2019.102391>
- Schlumberger D. (1984). *Cementing technology*. Nova Communications Limited.
- Singh, M., & Vander Wal, R. (2018). Nanostructure Quantification of Carbon Blacks. *C*, 5(1), 2. <https://doi.org/10.3390/c5010002>
- Sridhar, R., Aosai, P., Imjai, T., Setkit, M., Shirkol, A., & Laory, I. (2024a). Influence of nanoparticles and PVA fibers on concrete and mortar on microstructural and durability properties. *Fibers*. <https://doi.org/10.3390/fib12070054>
- Sridhar, R., Imjai, T., & Laory, I. (2024b). Experimental and numerical investigation of hybrid fiber reinforced concrete for vibration-based damage assessment. *Engineering Sciences*. <https://doi.org/10.30919/es1174>
- Webster, W. W., & Eikerts, J. V. (1979). Flow after cementing - a field and laboratory study. *Audio Eng Soc Preprint*. <https://doi.org/10.2523/8259-ms>
- Wu, J., Xie, S., Ji, Z., Wu, Z., Ma, C., & Wang, J. (2024). Effect of nano carbon black content and dispersibility on the properties of cement paste. *Proc Instit Civil Eng Trans*. <https://doi.org/10.1680/jtran.24.00026>
- Yetunde, S., & Ogbonna, J. (2011). Challenges and remedy for cementing of hpht wells in nigerian operation. *Soc Petrol Eng Nigeria Ann Int Conf Exhib*. <https://doi.org/10.2118/150751-ms>
- Young, J. F., & Hansen, W. (1986). Volume relationships for c-s-h formation based on hydration stoichiometries. *MRS Online Proceedings Library*, 85(1), 313. <https://doi.org/10.1557/PROC-85-3>

Publisher's Note

Springer Nature remains neutral with regard to jurisdictional claims in published maps and institutional affiliations.

Ahmed Ebied is an M.Sc. student in the Power Mechanical Engineering Department at Cairo University, specializing in applied wellbore cementing engineering. His research focuses on enhancing the mechanical characteristics of the cement sheath throughout the wellbore's lifetime by integrating innovative technologies. Currently, he works as a Wellbore Construction Fluids Engineer at Schlumberger, where he is responsible for improving cement slurry systems to address the challenges of onshore and offshore wellbore conditions for various clients.

Sherif Fakher is an assistant professor in petroleum and energy engineering at The American University in Cairo (AUC). He holds a bachelor's degree in petroleum and energy engineering from AUC, and a master's of science and PhD in petroleum engineering from Missouri University of Science and Technology. He has worked as a research assistant at Missouri University of Science and Technology and as a post-doctoral researcher at AUC in multiple research projects aiming to develop new technology to improve oil and gas recovery in a safe and cost effective manner while reducing the oil and gas industry's carbon footprint. His research resulted in the publication of more than forty technical papers and multiple awards worldwide.

Hatem Kayed is a seasoned academic and industry expert currently serving as an Associate Professor in the Power Mechanical Engineering Department at Cairo University. With a specialization in thermodynamics, combustion systems, and renewable energy, he leads the Combustion Group within the department. Dr. Kayed holds a Ph.D. in Power Mechanical Engineering from Cairo University, where he also completed his M.Sc. and B.Sc. studies. Beyond his academic role, Dr. Kayed is a dedicated consultant in Mechanical, Electrical, and Plumbing (MEP) systems and sustainable energy technologies. Dr.

Kayed has taught a variety of undergraduate and graduate courses such as Thermodynamics, Combustion Fundamentals, and Computational Fluid Dynamics. Known for his commitment to active learning, he employs diverse teaching techniques to engage students and improve their engineering skills. In research, Dr. Kayed has published over 30 research articles in leading journals and conferences, focusing on thermo-fluid dynamics, biofuels combustion, and spray and atomization. He has experience in conducting independent research, collaborating on projects, and mentoring students. His recent work includes advancements in clean combustion technologies, energy systems modeling, and solar desalination projects.